applied sciences

MDPI

Article

Thermodynamic Behavior of As, Pb, and As during the Vacuum Carbothermal Reduction of Copper Anode Slime

Juhai Deng [1,2,3], Guozheng Zha [1,2,3], Dachun Liu [1,2,3,4], Jilin He [3,5] and Wenlong Jiang [1,2,3,4,*]

1 Key Laboratory for Nonferrous Vacuum Metallurgy of Yunnan Province, Kunming 650093, China; dengjuhaily@163.com (J.D.)
2 National Engineering Research Center of Vacuum Metallurgy, Kunming University of Science and Technology, Kunming 650093, China
3 Faculty of Metallurgical and Energy Engineering, Kunming University of Science and Technology, Kunming 650093, China
4 State Key Laboratory of Complex Nonferrous Metal Resources Clean Utilization, Kunming University of Science and Technology, Kunming 650093, China
5 School of Material Science and Engineering, Zhengzhou University, Zhengzhou 450001, China
* Correspondence: wenlong_jiang@kust.edu.cn; Tel.: +86-15987187472

Abstract: The use of copper anode slime (CAS) for the removal of lead, bismuth, and arsenic is the key to recovering precious metals. In this paper, vacuum differential gravimetry experiments combined with thermodynamic equilibrium calculations reveal the effects of the temperature, system pressure, and carbon concentration on the interactions among Pb, Bi, and As during reduction. The carbon content is a direct factor limiting the reduction reactions of sulfate and arsenate phases, and affects the presence of arsenate reduction products. When the carbon content of the system is insufficient, As mainly exists as oxides in the reduction products, and the form of arsenic gradually converts to monomers with increasing carbon content. The reduction product Bi_2S_3 gradually converts to Bi and BiS as the temperature increases. The effect of temperature on arsenate is mainly related to the phase of the Pb- and Bi-containing reduction products. Moreover, vacuum differential gravimetry experiments were performed to verify the phase transformation of As, Pb, and Bi in CAS during vacuum carbon thermal reduction.

Keywords: copper anode slime; vacuum carbothermal reduction; thermodynamic equilibrium analysis; vacuum differential gravity method

Citation: Deng, J.; Zha, G.; Liu, D.; He, J.; Jiang, W. Thermodynamic Behavior of As, Pb, and As during the Vacuum Carbothermal Reduction of Copper Anode Slime. *Appl. Sci.* **2023**, *13*, 5878. https://doi.org/10.3390/app13105878

Academic Editors: Branislav Bul'ko, Mária Hagarová and Dana Baricová

Received: 12 April 2023
Revised: 26 April 2023
Accepted: 5 May 2023
Published: 10 May 2023

1. Introduction

Copper was one of the first metals processed by humans and has been an important material in the development of civilization. Copper has become a major industrial metal, ranking third after iron and aluminum in terms of quantities consumed. Copper anode slime (CAS) is an important industrial by-product generated at the bottom of electrorefining tanks during copper electrolytic refining, and contains significant amounts of gold, silver, selenium, tellurium, platinum-group precious metals and lead, bismuth, antimony, copper, and other valuable metals. Therefore, CAS is one of the main raw materials for the extraction of rare precious metals [1]. China is a major copper-producing and copper-consuming country. According to the United States Geological Survey, the global production of refined copper in 2021 was 26,000 billion tons, and China produced 10,000 billion tons of refined copper [2]. Almost all of China's known silver resources are associated with non-ferrous metals, of which lead and zinc deposits account for 51.4% and copper deposits account for 34.9% [3]. In the first quarter of 2022, raw gold production within China reached 83.401 tons, of which 65.009 tons was mineral gold and 18.392 tons was non-ferrous by-product gold [4]. The production of copper, lead, and other non-ferrous metals is steadily growing, and the by-products of their refining processes have become important raw materials for the

extraction of gold, silver, and other valuable metals [5]. Table 1 lists the composition of CAS from various refineries and regions. The high contents of heavy metals in CAS indicate that it is an important raw material for the extraction of precious metals [6]. On one hand, the recovery of metals from CAS can bring considerable economic benefits. On the other hand, CAS is a kind of hazardous waste, in which heavy metals such as Cd, Pb, and As may cause an environmental and ecological threat [7]. Therefore, it is necessary to develop novel green technologies for PMs recovery from CAS with the constraints of environmental regulations and the requirements in revenue increase. The key to all methods is to achieve the separation of precious metals (gold, silver, etc.) from valuable metals (lead, bismuth, etc.).

Table 1. Composition of CAS from various refineries (wt. %).

Resource	Ag	Au	As	Pb	Bi
La Caridad Copper Refinery [8]	15.4	0.04	5.00	14.80	1.20
Qinghai Copper Industry Co. [9]	5.00	0.15	2.12	28.5	4.61
Sarkuysan Copper, Turkey [5]	2.80	0.23	3.93	12.93	0.15
Medium-scale copper smelter in western China [10]	5.36	0.16	2.38	28.65	3.86
Yunnan [11]	4.79	0.18	6.21	3.18	3.15
Toyama, Japan [12]	17.00	1.04	0.41	35.10	–
Tehran, Iran [13]	7.07	0.08	0.42	4.42	0.08
Noranda (Canada) [14]	19.50	0.18	1.14	8.00	0.77
IMI Refinery (UK) [14]	5.50	0.07	3.50	22.00	0.50
INCO (USA) [14]	6.37	0.12	0.50	1.70	0.14
La Caridad Copper Refinery (Mexico) [8]	15.40	0.04	5.00	14.80	1.20
Rio Tinto Minera Copper Refinery, Huelva (Spain) [15]	14.54	0.38	3.41	2.89	0.76

The prominent approaches that have been developed to treat CAS include the traditional pyrometallurgical process, combined Kaldor furnace dressing–metallurgy method, hydrometallurgical methods, and combined pyrometallurgical and hydrometallurgical half-wet method. The pyrometallurgical process is currently the mainstream process because of its large processing capacity and strong adaptability to a variety of raw materials. First, a precious metal lead alloy is produced by high-temperature reduction smelting. Subsequently, the obtained alloy is oxidized and smelted to remove Pb and produce a Au–Ag–Pt alloy. Finally, Ag and Au are obtained by electrolysis. However, this method is usually characterized by high energy consumption, low purity of the recovered Ag, and air pollution during recycling (including SO_2, PbO, As_2O_3, and Sb in the soot). In recent years, an improvement to the traditional firing process, i.e., the Kaldor furnace process [16], as well as the vacuum distillation process were developed. The Kaldor furnace process is used to complete the reduction and oxidation of anode slime in a Kaldor furnace. This method has advantages such as equipment processing capacity, short operation time, less metal backlog, low energy consumption, small amount of flue gas, and good operating environment. However, the equipment investment is high, and the furnace charge return volume increases the cost of late slag treatment [16,17].

A previous study developed an integrated hydrometallurgical process consisting of leaching, solvent extraction, and cementation. The leaching agent was HCl + H_2O_2, and the extractants included Cyanex272 and LIX 63. The overall recoveries of Au and Ag from anode slime were 91.4% and 96.9%, respectively [18]. An oxidative pretreatment–thiosulfate leaching–electrodeposition process was employed, which avoided the emission of harmful gases, such as sulfur dioxide and ammonium; the maximum recovery of Ag using this process was 95.4%. However, both these methods have challenges, such as a long metal recovery cycle and difficulty in treating acid-containing wastewater [1].

Furthermore, a pyro-hydrometallurgical process [10], sulfation roasting–water adsorption, was proposed to treat CAS, and was first conducted to recover selenium. Subsequently, water leaching–iron powder cementation was adopted to extract Cu from the roasted residue. Afterwards, selective chloride leaching–$H_2C_2O_4$ reduction was applied to

extract Au from the copper-leaching residue. Finally, sulfite leaching–$Na_2S_2O_4$ reduction was employed to recover Ag from the gold-leaching residue, and the barren leachate was recycled for use in silver leaching with the addition of a small quantity of lixiviant. The use of this integrated pyro-hydrometallurgical process resulted in recovery yields of 98.7% of Au, 98.6% of Ag, and 99.8% of Pb from the mud.

In the traditional pyrometallurgical process, Pb, Bi, As, and other base metals are mainly removed during oxidation refinement in a silver separation furnace. This removal depends on the different affinities of each metal element for oxygen to enable sequential oxidation, subsequent transfer into the slag or dust, and separation from the precious metals [19]. However, this process generates a large amount of soot and precious metal-containing slag. Therefore, vacuum distillation was introduced to replace the oxidation-blowing process of precious metals in the traditional firing method; since then, it has also been industrially applied [20]. This process relies on the difference in physicochemical properties between base metals and noble metals to volatilize the group with a higher vapor pressure in order to enrich the noble metals. However, anode slime with a high arsenic content will produce a high concentration of arsenic oxide fume during smelting, which can cause serious and irreversible damage to the environment and human health [21].

Arsenic emission has always been a challenge for lead and copper smelting enterprises. Arsenic continually accumulates in each step of the traditional pyrometallurgical process and has not been effectively opened up [22]. The current pyrometallurgical process uses reduction melting, which inevitably generates arsenic oxide fume and dust. Therefore, this paper we used a vacuum carbothermal reduction method to treat anode slime. During the low-temperature vacuum carbothermal reduction, arsenic is volatilized as arsenic oxide and recovered as volatiles, and no soot is generated in the process. The arsenic content in the residue was reduced from 9.35% to 0.48%, realizing 94.89% arsenic removal [23]. The whole process is performed in a closed environment, providing a new strategy for the green and efficient recycling of CAS [24]. However, the evolution of arsenic throughout the process and the underlying mechanisms are not yet clear. Therefore, this study elucidates the evolution of arsenic during the vacuum thermal reduction of CAS using a vacuum thermogravimetric furnace combined with FactSage thermodynamic simulations [25]. Furthermore, additional thermodynamic data for the carbothermal reduction of CAS under vacuum conditions are provided and the underlying mechanism is elucidated to provide a theoretical basis for industrial production.

2. Materials and Methods

2.1. Sample Preparation and Characterization

Copper anode slime was kindly provided by a copper smelter in Yunnan, China. First, the CAS was crushed by a crusher and then passed through 300 mesh sieves. A representative sample was obtained, which was analyzed for Ba, S, Fe, Cu, Pb, Bi, Zn, Au, Ag, and other elements. The chemical composition of the dry anode slime was measured using inductively coupled plasma atomic emission spectroscopy (ICP-AES, OPTIMA 8000, PerkinElmer, America), chemical analysis, inductively coupled plasma atomic absorption spectroscopy (AAS, WFX-320, Beijing Beifen-Ruili, China), and X-ray fluorescence spectrometer (XRF, Bruker S6 Jaguar, Germany), and the data are listed in Table 2.

Table 2. Chemical composition of the raw materials (* O content obtained by XRF).

	Element	Ag	Au (g/t)	Bi	Pb	As	Ba	S	O *
Raw materials	Content (wt. %)	5.24	927.9	12.92	12.1	9.35	7.64	6.94	15.52
	Element	Sb	Te	Se	Cu	Ni	Fe	Zn	
	Content (wt. %)	4.94	1.64	0.71	0.7	0.41	0.27	0.007	

The phase of the raw material was analyzed using X-ray diffraction (XRD, D-MAX/2600, Rigaku, Japan) (Figure 1), and the components in the anode slime were mainly Ag, $PbSO_4$, $Pb_3(AsO_4)_2$, $Pb_2As_2O_7$, $Bi_2(SO_4)_3$, $BiAsO_4$, As_2O_3, $BaSO_4$, Sb_2O_3, Sb_2O_3, and SiO_2. The morphology and elemental distribution of the CAS were analyzed with scanning electron microscopy (SEM, ZEISS Gemini SEM 300, Germany). The SEM results showed a clear overlap of Pb- and Bi-enriched areas. This implies that the physical phase of Bi-containing compounds is similar to that of lead-containing ones. The distribution of Au was relatively uniform and did not overlap with those of the other elements. Combined with the XRD results, the presence of the corresponding arsenate phase was also demonstrated. Pb-enriched and S-enriched regions overlapped, confirming the presence of the lead sulfate phase.

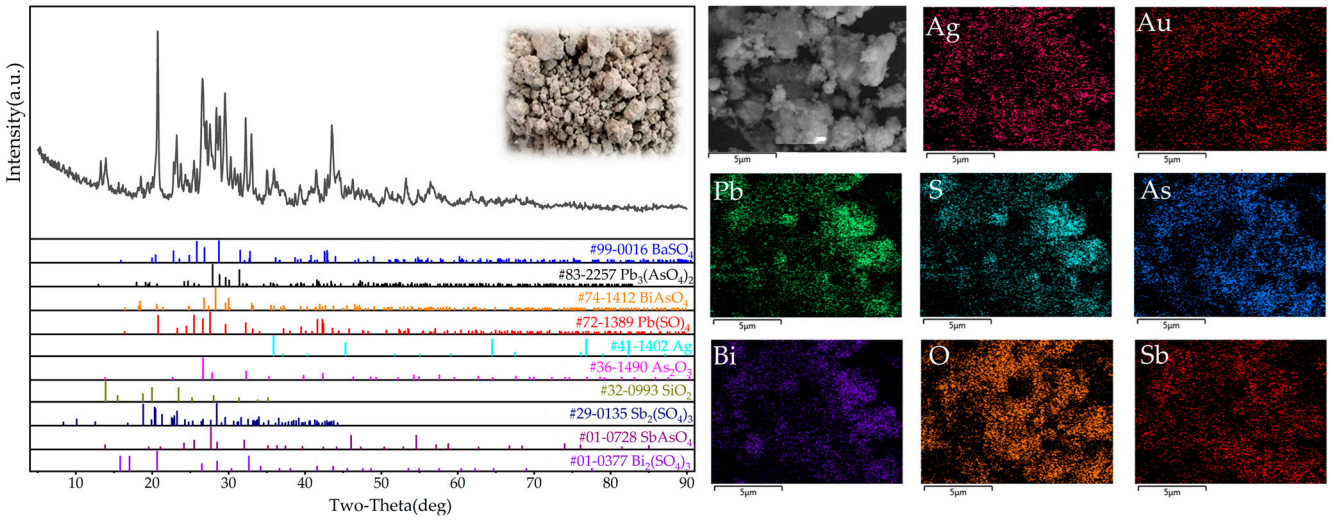

Figure 1. XRD pattern and SEM–EDS images of CAS.

2.2. Vacuum Thermogravimetry Tests

The raw material was mixed with charcoal powder (fixed carbon content of 67 wt. %) at 30 wt. % of the mass of the anode slime, following which sufficient binder (5 wt. % of raw material) was added to enable palletization. The prepared pellets containing carbon were dried in a drying oven. During the experiment, 15 g of pellets were placed in the vacuum thermogravimetric furnace, and the vacuum system was stabilized. The weight loss of the raw material was recorded by controlling different temperature conditions. The material phase was detected at the end of the experiment. Figure 2 illustrates the relevant experimental ideas.

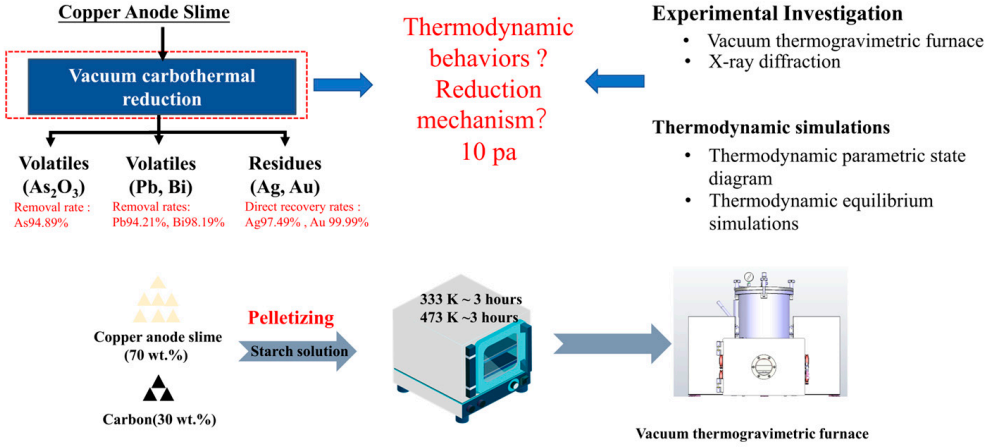

Figure 2. Experimental idea chart.

The vacuum thermogravimetric furnace used in the experiments collects one sample point of data including the sample weight, temperature, and system pressure every second, which is developed by the National Engineering Research Center of Vacuum Metallurgy. Structural diagrams are shown in Figure 3. The device can provide information about the occurrence of chemical reactions via mass changes under vacuum conditions in real time by recording changes in the crucible weight and temperature. It is also possible to determine the evaporation rate of a substance under specific conditions.

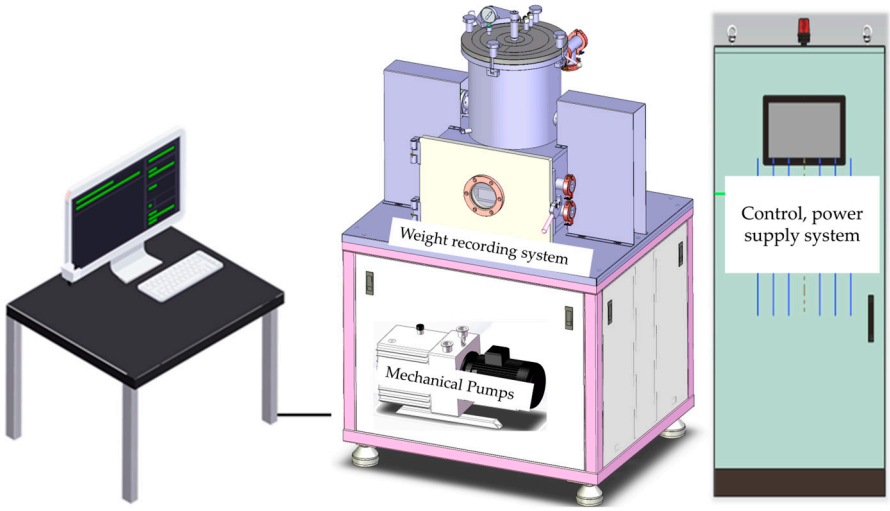

Figure 3. Schematic of the experimental equipment.

The combination of a mechanical pump and an external gas supply allowed the pressure in the furnace to be maintained at a desired fixed value. The range of the system pressure could be controlled from 1 Pa to 10.1 kPa. Current was applied to a graphite resistance element that was used to heat the crucible in the vacuum thermogravimetric furnace. The temperature inside the furnace could be controlled from 300 to 1873 K, with a precision of 1 K.

2.3. Thermodynamic Simulations

To clarify the phase changes and elemental distribution in the vacuum carbothermal reduction process of CAS, we used the equilibrium module in FactSage 7.2 for thermodynamic simulations. The module is based on the minimum Gibbs free energy principle of calculation, and the FactPS database was used. The input phases were $PbSO_4$, $Pb_3(AsO_4)_2$, $Bi_2(SO_4)_3$, $BiAsO_4$, and C. The system pressure was 10 Pa. The development of a thermodynamic parametric state diagram based on a large amount of thermodynamic balance data provides a simple and intuitive thermodynamic analysis method and reveals the relationship between the differential thermodynamic parameters and the state of the system. The Phase Diagram module [26] and the Predom module in FactSage 7.2, as well as the FTdemo and FactPS databases, were used to obtain phase diagrams and dominant area diagrams (PADs) [27] for various systems under different conditions.

3. Results

3.1. Thermodynamic Equilibrium Simulations

The PADs of the Pb–As–O–C, Bi–As–O–C, Pb–S–O–C, and Bi–S–O–C systems are shown in Figure 4. For the arsenate system (Figure 4a,b), the reaction starts with arsenic oxide as a reduction product with a very low starting partial pressure. In addition, the system is under vacuum and the partial pressure of oxygen is also very low; hence, the stable state of the metal element in this state should be an oxide or monomer. The sulfate system

(Figure 4c,d) is similar to the arsenate system sulfur dioxide system, as a reduction product is not present in the system at the beginning of the reaction and that the starting partial pressures are low, with the difference being that the stable state of the metallic element is either an oxide, sulfide, or monomer. Therefore, the reactions shown in Equations (1)–(5) may occur under vacuum conditions.

$$Me_x(AsO_4)_y + C \rightarrow Me + As_2O_3 \quad (1)$$

$$Me_x(AsO_4)_y + C \rightarrow Me_xO_y + As_2O_3 \quad (2)$$

$$Me_x(SO_4)_y + C \rightarrow Me_xS_y \quad (3)$$

$$Me_x(SO_4)_y + C \rightarrow Me_xO_y \quad (4)$$

$$Me_x(SO_4)_y + C \rightarrow Me \quad (5)$$

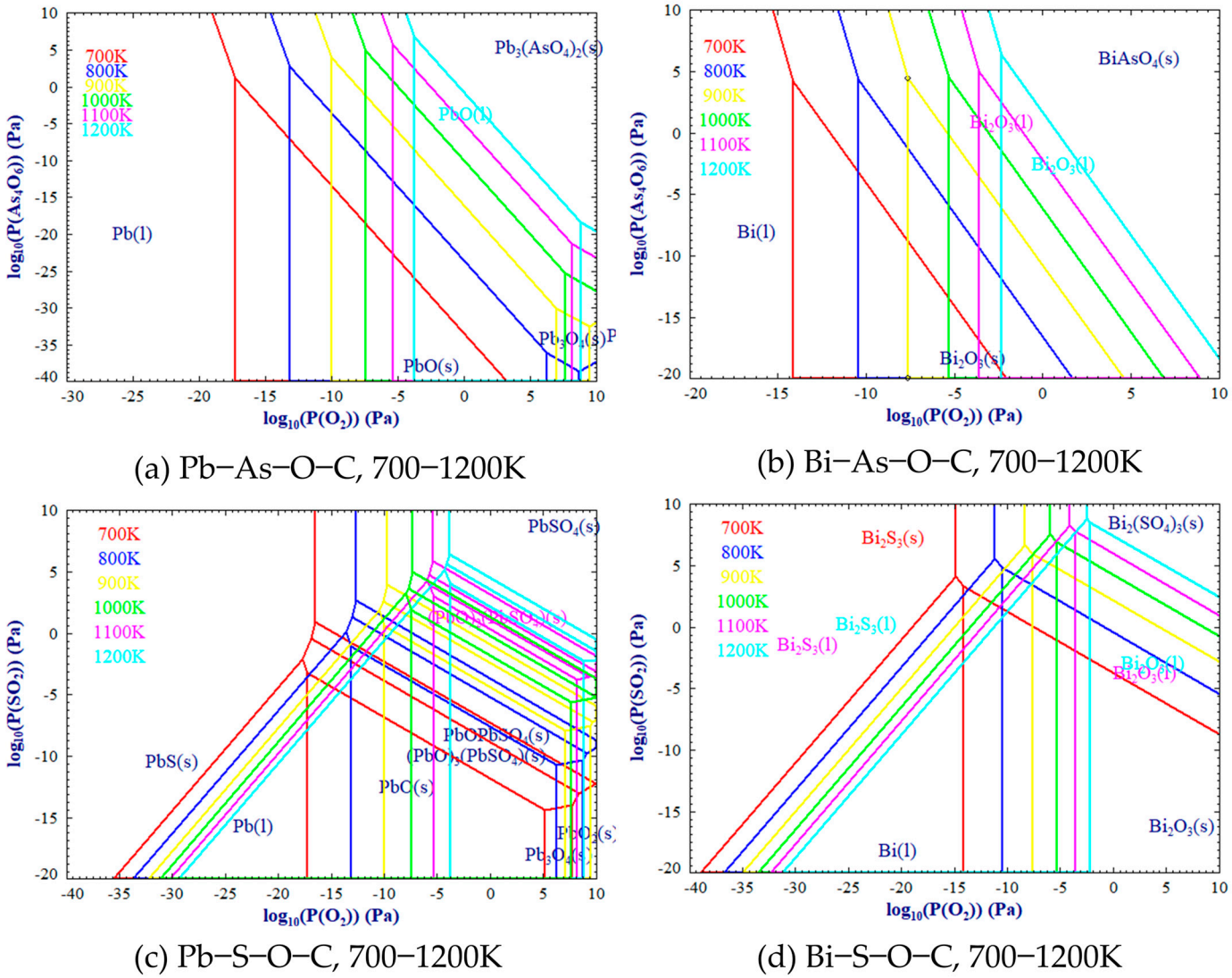

Figure 4. Two-dimensional PADs for arsenate and sulfate systems at different temperatures (fixed system pressure of 10 Pa).

Figures 5 and 6 shows the transformation behaviors of CAS during the vacuum carbothermal reduction simulated by FactSage 7.2. We discuss the trends in the elemental

morphology of the main substances in the raw material under vacuum carbothermal reduction conditions (10 Pa) with increasing carbon content.

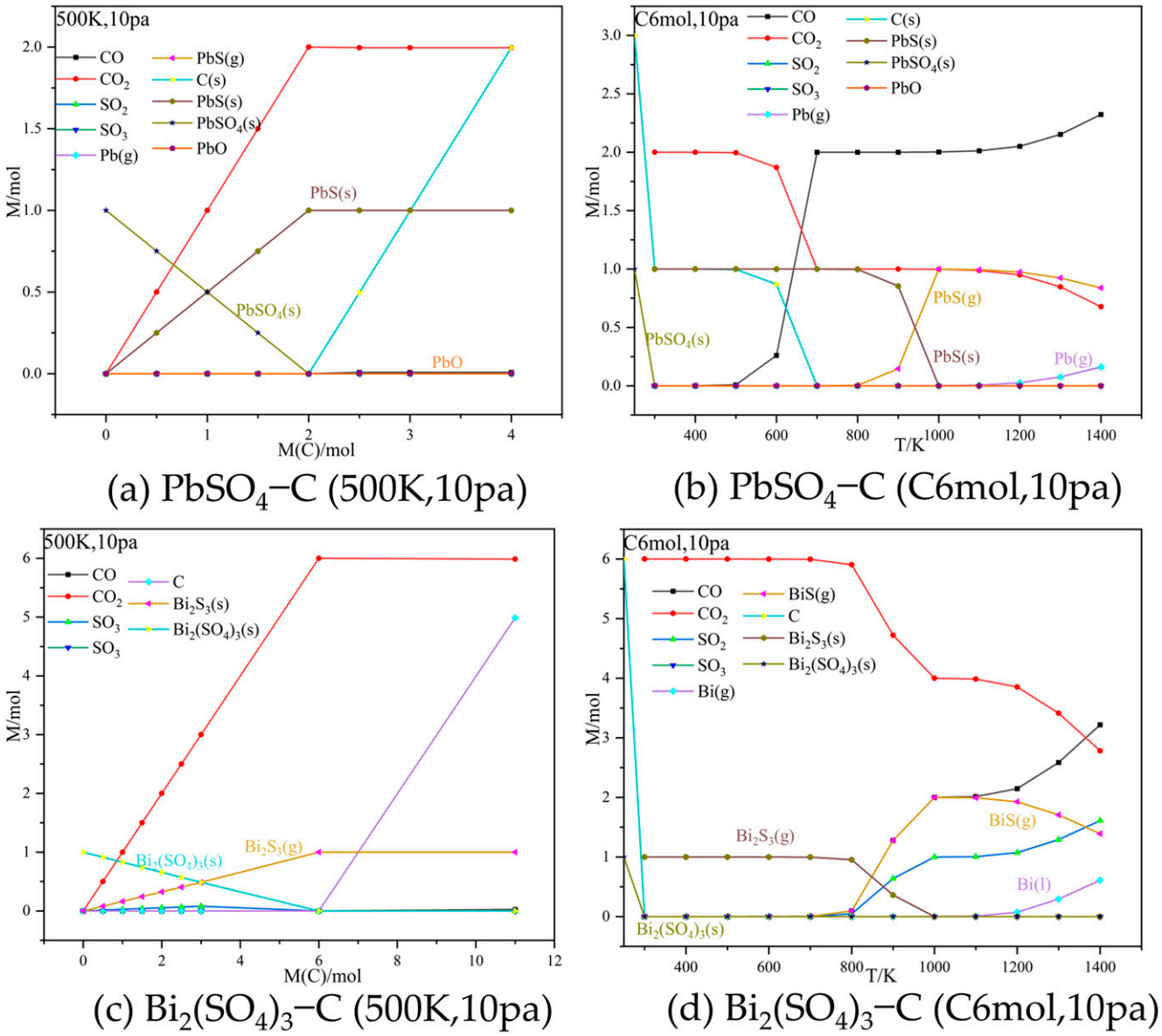

Figure 5. Transformation behavior of $PbSO_4$, $Bi_2(SO_4)_3$, and C during vacuum carbothermal reduction.

First, under the simulated conditions, $PbSO_4$ does not decompose, but the reduction reaction occurs with increasing carbon content in the system. The product is PbS, with no lead-oxide phase present. Figure 5a shows the effect of different temperatures with a guaranteed excess of carbon in the system. When the carbon content in the system is sufficient, the starting temperature of the vacuum carbothermal reduction reaction of $PbSO_4$ is very low and the temperature only affects the presence of the PbS product. Only when the temperature exceeds 1200 K does elemental lead appear. The $Bi_2(SO_4)_3$ system is similar to $PbSO_4$ in that under the simulated conditions, $Bi_2(SO_4)_3$ does not decompose and undergoes a reduction reaction with increasing carbon content in the system, to yield the product Bi_2S_3. With an excess of carbon in the system, the product Bi_2S_3 is gradually replaced by Bi and BiS as the temperature increases, as shown in Figure 5d.

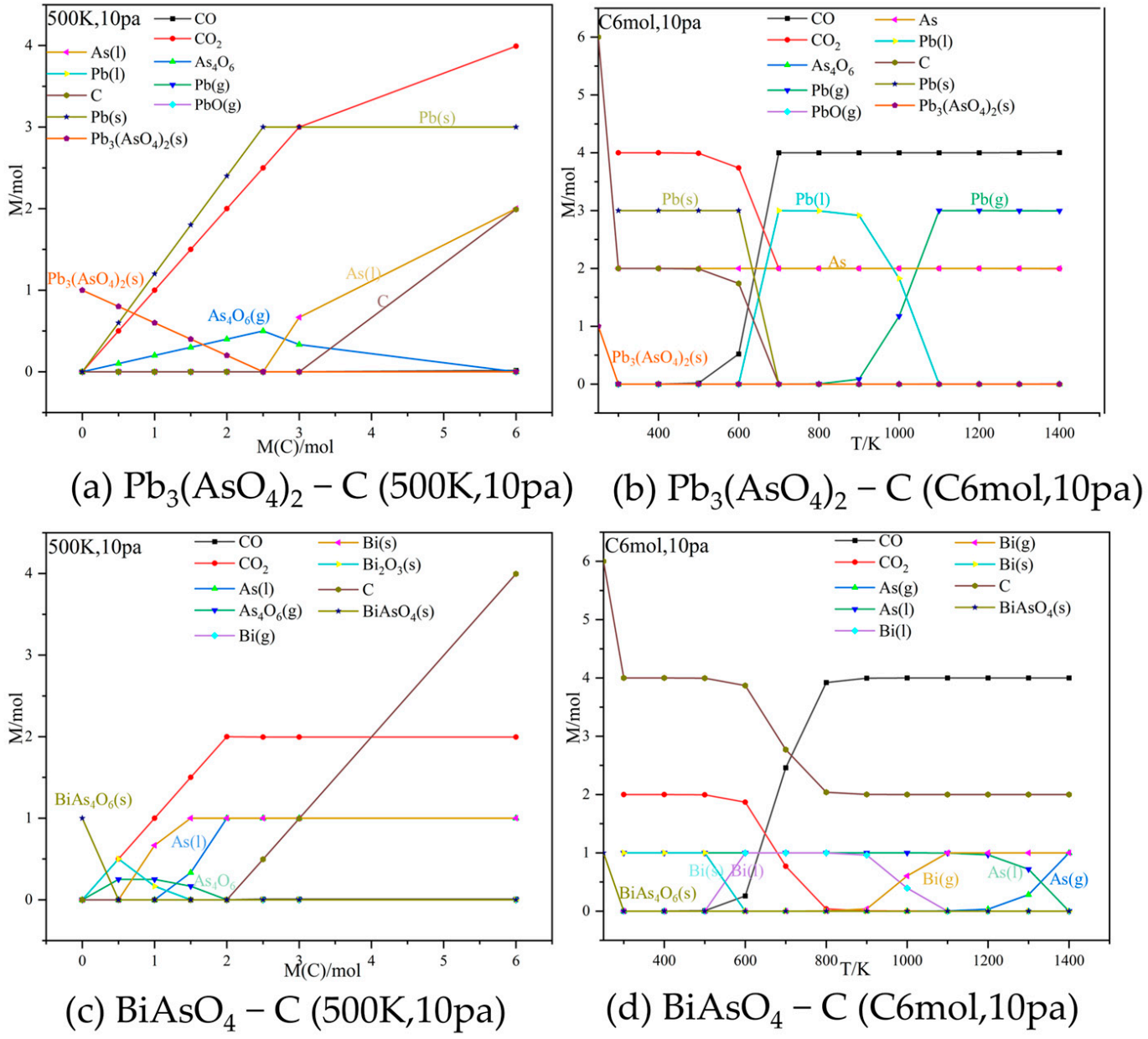

Figure 6. Transformation behavior of $Pb_3(AsO_4)_2$, $BiAsO_4$, and C during vacuum carbothermal reduction.

The $Pb_3(AsO_4)_2$ system is more complex than those mentioned previously, and $Pb_3(AsO_4)_2$ has a higher thermal decomposition temperature under vacuum conditions. However, the temperature required for vacuum carbothermal reduction is lower, and the main As phases in the product are elemental arsenic and arsenic oxide, while Pb is present as elemental lead. Figure 6a shows the transition of As from the arsenic oxide phase to elemental As as the carbon content of the system increases. In the case of excess carbon in the system, the temperature only has an effect on the state of the elemental Pb and As products. The $BiAsO_4$ system is similar to the $Pb_3(AsO_4)_2$ system in that the vacuum thermal decomposition temperature is higher than that for the others. Figure 6c shows that insufficient system carbon can lead to the generation of some Bi and As in the form of oxides. In the case of excess carbon, the temperature only has an effect on the state of the Pb and As products.

3.2. Vacuum Carbothermal Reduction

Based on the previous theoretical analysis, the removal of As from the feedstock mainly occurred around 723 K and was mainly caused by the decomposition of arsenate. However, the changes in the fugitive form of As during As removal are not clear. Therefore, the temperature range of the experiment was set at 300–723 K, and the heating rate was set to 2–5 K/min to ensure the accuracy of the experiment. The weight-loss and temperature profiles of the material are shown in Figure 7a, and the XRD pattern of the residue remaining at the end of the experiment is shown in Figure 7b.

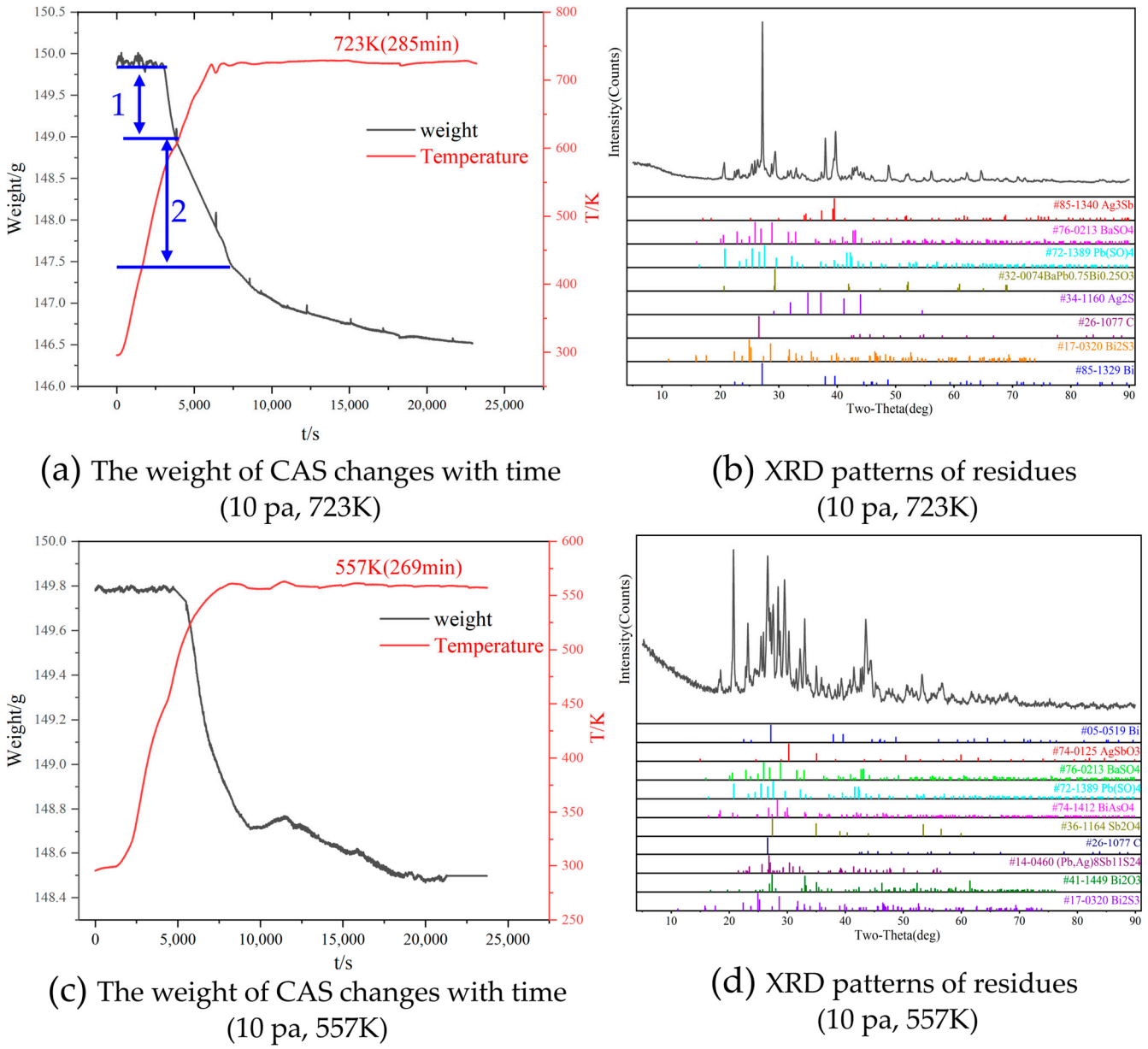

Figure 7. Vacuum thermogravimetry experimental results.

Figure 7a shows two weight-loss plateaus. We believe that under vacuum conditions, there is no material exchange between the system and the external environment, which means that during the experimental process, there will be no weight gain during the differential weight experiment without the addition of external substances, Therefore, the fluctuating changes in weight in Figure 4a at the beginning of the experiment and the sudden increase in weight during the experiment are caused by experimental errors.

Because of the high precision of the weighing system, changes in the system pressure cause a change in the scale reading; hence, the mass increase is considered an error caused by the change in the system pressure. The entire curve is divided into two weight-loss stages, the first starting at a temperature of ~557 K and the second at ~723 K. The XRD results of the residue showed that under the experimental conditions, lead arsenate and bismuth arsenate phases are not present in the residue, but the metallic Bi phase is observed. According to previous thermodynamic simulation results, it is known that the metallic Bi phase will not appear in the reduction reaction of bismuth sulfate under the experimental conditions; hence, the metallic Bi phase was formed by the thermal reduction of bismuth arsenate. The presence of sulfate phases in the residue may be due to incomplete sulfate reduction owing to an insufficient reaction time. It was initially determined that the weight losses during the experiments were mainly caused by the thermal reduction of arsenate and product volatilization.

To further investigate the phase changes in each weight-loss section, we refined the experimental parameters and performed experiments with a heating rate of 2–3 K/min. Under these conditions, the first weight-loss temperature shifted from 557 K (Figure 7c) to ~500 K, and the second weight loss started at ~600 K (Figure 7a). Therefore, experiments were conducted to verify the material phases present at 500 and 600 K.

According to Figure 8b, it can be seen that at the beginning of the reaction, bismuth sulfate will first react with lead arsenate to form lead sulfate and bismuth arsenate. The disappearance of the bismuth sulfate phase in the residue at 500 K (Figure 8a) also proves that bismuth sulfate and lead arsenate reacted to form lead sulfate and bismuth arsenate. According to the thermodynamic equilibrium simulation results of the mixture, the system should not contain bismuth sulfide, but the XRD results in Figure 8b identified $Pb_2Bi_6S_{11}$ in the residue. Figure 8c shows the effect of different carbon content and system pressure on the M system. The amount of carbon content directly affects the amount of sulfate/arsenate reduction. The experiments were carried out in the presence of carbon excess and the sulfate was reduced to monomers and metal sulfides at 500 K. Arsenate was then reduced to monomers. The system pressure directly affects the size of the corresponding reduction product stabilization zone. Only when the carbon content of the system is insufficient, arsenic exists in the form of oxides. Comparing Figure 8c,f, the increase in temperature reduces the stable presence phase of sulfate/arsenate and expands the phase of reduction products. There is little effect on the type of reduction products.

According to the results of the thermodynamic equilibrium simulations, the amount of carbon added directly affects the presence of Bi and As in the reduction products; bismuth oxide and arsenic oxide are generated when carbon is insufficient. The presence of the C phase in the residue proves that the experiments were performed with excess carbon; it is also clear from the simulation results that the oxide phase does not appear in this case. However, oxide phases are present in the experimental product. This is because the saturation vapor pressure of arsenic oxide is greater than that of monolithic arsenic, and during vacuum carbothermal reduction, As is volatilized preferentially in the form of arsenic oxide. In contrast, the saturation vapor pressure of bismuth oxide is much lower than that of bismuth sulfide and monolithic bismuth, and due to the lack of carbon around some of the bismuth sulfate at the beginning of the reaction, bismuth oxide is generated preferentially and remains in the residue.

The product phase at 600 K (Figure 8e) is similar to that at 500 K (Figure 8a), and the thermodynamic equilibrium simulation results are also similar; the difference is that when the temperature is 600 K, with the increase of C content, some CO_2 will react with C to generate CO. In addition, the generated CO can reduce Bi_2O_3 to Bi (600 K, reaction Gibbs free energy: −288.316 kJ), which also explains why Bi_2O_3 is present at 500 K but not at 600 K.

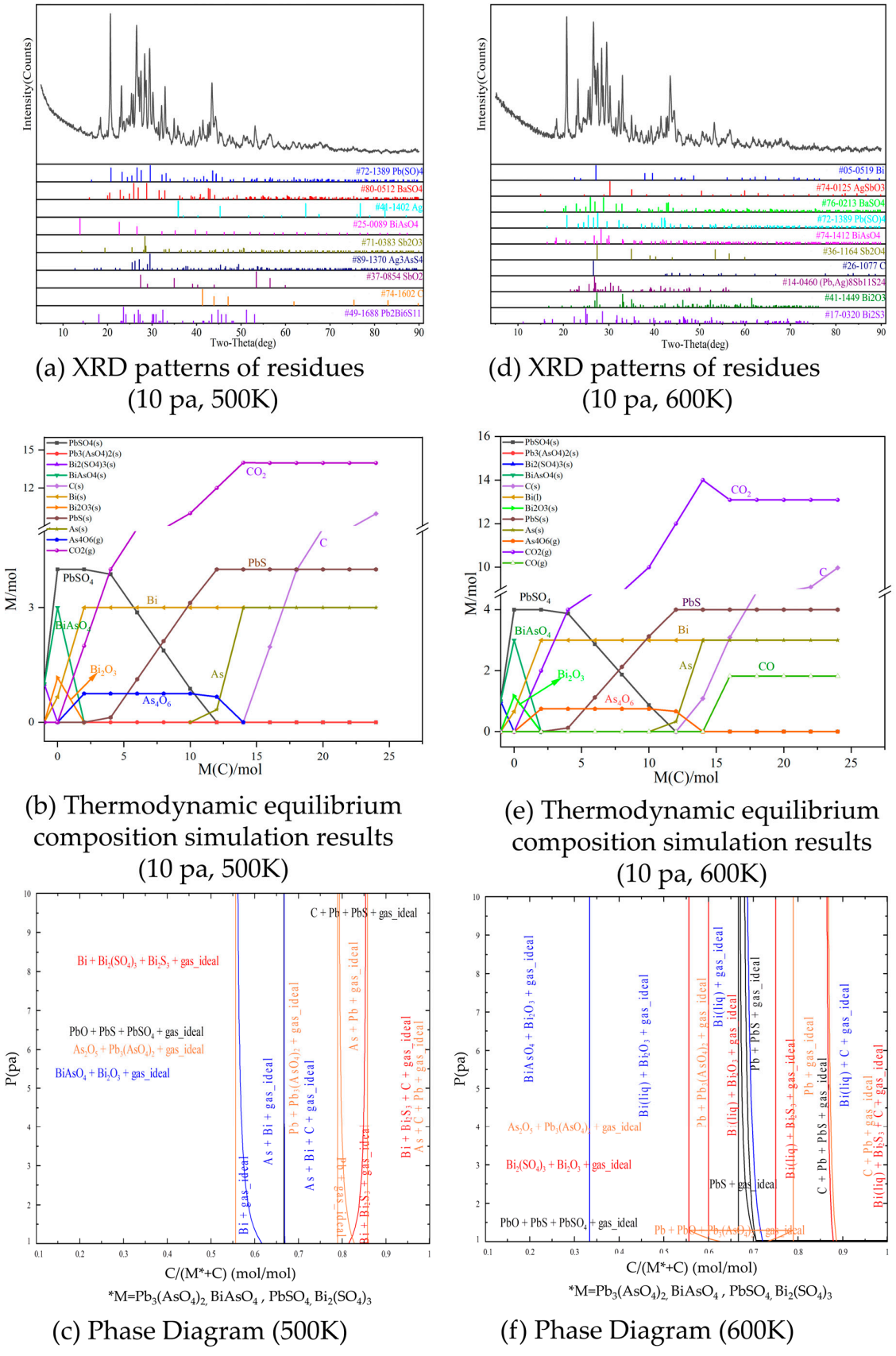

Figure 8. Thermodynamic simulation results and XRD patterns of products at different temperatures.

Therefore, the reactions that occur throughout the vacuum carbothermal reduction process are mainly those described by Equations (6)–(9). The reduction product of lead arsenate, i.e., the lead monomer, was not detected in the residue, but the original lead arsenate phase disappeared. This indicates the reaction of lead arsenate with bismuth sulfate in the raw material to form lead sulfate and bismuth arsenate. Lead sulfide and bismuth sulfide were detected in the residue, which indicates that the further reduction of lead sulfate and bismuth sulfate occurred. In addition, the presence of the monomeric bismuth phase in the residue indicates that bismuth arsenate was reduced.

$$Pb_3(AsO_4)_2 + Bi_2(SO_4)_3 = 3PbSO_4 + 2BiAsO_4 \quad (6)$$

$$4BiAsO_4 + 5C = 4Bi + 5CO_2 + 2As_2O_3 \quad (7)$$

$$PbSO_4 + 2C = PbS + 2CO_2 \quad (8)$$

$$Bi_2(SO_4)_3 + 6C = Bi_2S_3 + 6CO_2 \quad (9)$$

Figure 9a,b show XRD patterns of the volatiles condensed near the mouth of the graphite crucible and the furnace cover. The experimental raw materials contained arsenic oxide and antimony oxide, and arsenic oxide and antimony oxide were detected in the volatiles. This indicates that the volatile behavior of volatile components was also accompanied by the vacuum carbon thermal reduction process. The presence of PbS and $Pb_2Bi_2S_5$ phases in the volatiles confirms the successful vacuum carbothermal reduction of lead sulfate and bismuth sulfate. The presence of the bismuth phase in the volatiles indicates the successful vacuum carbothermal reduction of bismuth arsenate. The detection of the reduction product phase in the volatiles also indicates that the entire vacuum carbothermal reduction process is accompanied by a reduction reaction and volatilization of volatile components.

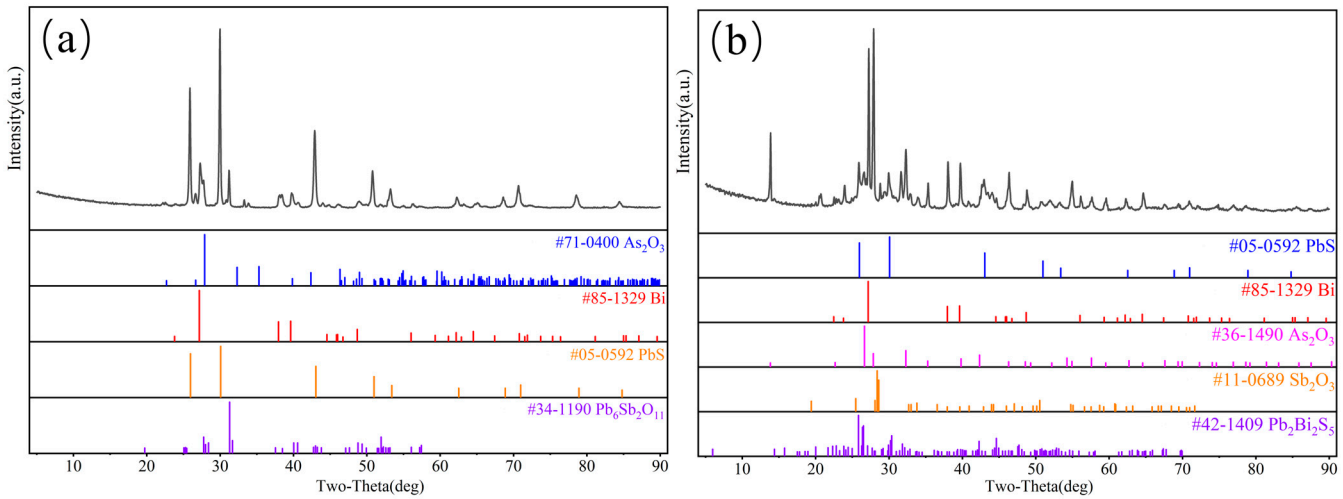

Figure 9. (**a**) XRD patterns of volatiles collected near the mouth of the graphite crucible, (**b**) XRD patterns of volatiles collected at the furnace cover.

4. Conclusions

From the thermodynamic simulation results, under the condition that carbon is always in excess in the vacuum carbothermal reduction of CAS, the following reactions mainly occur: $Pb_3(AsO_4)_2 + Bi_2(SO_4)_3 = 3PbSO_4 + 2BiAsO_4$; $4BiAsO_4 + 5C = 4Bi + 5CO_2 + 2As_2O_3$; $PbSO_4 + 2C = PbS + 2CO_2$; $Bi_2(SO_4)_3 + 6C = Bi_2S_3 + 6CO_2$.

When the carbon content of the system was insufficient, the arsenic in the reduction products mainly existed as oxides, and the arsenic phase gradually converted to monomers with increasing carbon content.

From the results of vacuum differential gravimetric experiments, the process of carbothermal reduction under vacuum at 10 Pa and 300–723 K was always accompanied by the volatilization of volatile components from the raw material and reduction products. The reduction product of lead arsenate (lead monomer) was not detected in the residue, but the lead arsenate phase disappeared, indicating the reaction of lead arsenate with bismuth sulfate from the raw material to form lead sulfate and bismuth arsenate. The disappearance of the arsenate phase from the CAS indicates that it was successfully reduced. The detection of PbS and $Pb_2Bi_2S_5$ phases in the volatiles confirmed the successful reduction of lead sulfate and bismuth sulfate. However, the presence of lead sulfate in the residue indicated that the sulfate reduction reaction was not complete.

In summary, the vacuum carbothermal reduction of CAS at 10 Pa and 300–723 K is thermodynamically feasible, but the specific reduction effect is also affected by the kinetics; therefore, further experiments are required to study the specific reduction kinetics of this system.

In this work, the change law of elements in the process of CAS vacuum carbothermal reduction was obtained through a combination of thermodynamic simulation calculation and experimental verification, but the kinetics of the process was not solved. The next work will carry out relevant kinetic research, expand the scale of experiments on the basis of thermodynamic and kinetic research, and provide theoretical support for subsequent industrial production.

Author Contributions: Conceptualization, J.D. and W.J.; methodology, J.D. and W.J.; investigation, J.D.; resources, D.L. and J.H.; writing—original draft preparation, J.D.; writing—review and editing, J.D., G.Z. and W.J.; funding acquisition, W.J. All authors have read and agreed to the published version of the manuscript.

Funding: This research was funded by The Fund of the National Natural Science Foundation of China, grant number 52064029, the national Key R&D Program, grant number 2022YFC2904900), Yunnan Science and Technology Plan Project, grant number 202102AB080014, 202201BE070001-056, the Scientist Studio of Yunnan Province.

Data Availability Statement: Not applicable.

Acknowledgments: The authors sincerely acknowledge the anonymous reviewers for their insights and comments, which further improved the quality of the manuscript.

Conflicts of Interest: The authors declare no conflict of interest.

References

1. Xiao, L.; Wang, Y.L.; Yu, Y.; Fu, G.Y.; Han, P.W.; Sun, Z.H.I.; Ye, S.F. An Environmentally Friendly Process to Selectively Recover Silver from Copper Anode Slime. *J. Clean. Prod.* **2018**, *187*, 708–716. [CrossRef]
2. United States Geological Survey. Available online: https://pubs.usgs.gov/periodicals/mcs2022/mcs2022-copper.pdf (accessed on 16 March 2023).
3. Bin, W.; Lu, Y. *Gui Jin Shu Ye Jin Xue*; Central South University Press: Changsha, China, 2011; ISBN 978-7-5487-0223-8.
4. China Gold Association in the First Quarter of 2022, Raw Gold Production within China Reached 83.401 Tons, of Which 65.009 Tons Was Mineral Gold and 18.392 Tons. Available online: http://www.cngold.org.cn/newsinfo.aspx?ID=3632 (accessed on 1 December 2022).
5. Kilic, Y.; Kartal, G.; Timur, S. An Investigation of Copper and Selenium Recovery from Copper Anode Slimes. *Int. J. Miner. Process.* **2013**, *124*, 75–82. [CrossRef]
6. Xing, W.D.; Sohn, S.H.; Lee, M.S. A Review on the Recovery of Noble Metals from Anode Slimes. *Miner. Process. Extr. Metall. Rev.* **2020**, *41*, 130–143. [CrossRef]
7. Zhu, W.; Zhu, N.; Xian, J.; Xi, Y.; Li, F.; Wu, P.; Chen, Y. A Green Process for Simultaneously Efficient Base Metals Removal and Precious Metals Enrichment from Copper Anode Slime. *Resour. Conserv. Recycl.* **2022**, *180*, 106200. [CrossRef]
8. Chen, T.T.; Dutrizac, J.E. Mineralogical Characterization of a Copper Anode and the Anode Slimes from the La Caridad Copper Refinery of Mexicana de Cobre. *Metall. Mater. Trans. B Process Metall. Mater. Process. Sci.* **2005**, *36*, 229–240. [CrossRef]
9. Dong, Z.; Jiang, T.; Xu, B.; Yang, J.; Chen, Y.; Li, Q.; Yang, Y. Comprehensive Recoveries of Selenium, Copper, Gold, Silver and Lead from a Copper Anode Slime with a Clean and Economical Hydrometallurgical Process. *Chem. Eng. J.* **2020**, *393*, 124762. [CrossRef]

10. Xu, B.; Chen, Y.; Dong, Z.; Jiang, T.; Zhang, B.; Liu, G.; Yang, J.; Li, Q.; Yang, Y. Eco-Friendly and Efficient Extraction of Valuable Elements from Copper Anode Mud Using an Integrated Pyro-Hydrometallurgical Process. *Resour. Conserv. Recycl.* **2021**, *164*, 105195. [CrossRef]
11. Wang, S.; Li, L.; Wang, S.D.; Wang, H.; Wu, G.D. Extraction of Platinum and Gold from Copper Anode Slimes by a Process of Chlorinating Roasting Followed by Chlorinating Leaching. *J. Min. Metall. Sect. B Metall.* **2020**, *56*, 15. [CrossRef]
12. Sanuki, S.; Minami, N.; Arai, K.; Izaki, T.; Majima, H. Oxidative Leaching Treatment of Copper Anode Slime in a Nitric Acid Solution Containing Sodium Chloride. *Mater. Trans. JIM* **1989**, *30*, 781–788. [CrossRef]
13. Khanlarian, M.; Rashchi, F.; Saba, M. A Modified Sulfation-Roasting-Leaching Process for Recovering Se, Cu, and Ag from Copper Anode Slimes at a Lower Temperature. *J. Environ. Manag.* **2019**, *235*, 303–309. [CrossRef] [PubMed]
14. Lee, J.; Kurniawan, K.; Chung, K.W.; Kim, S. Metallurgical Process for Total Recovery of All Constituent Metals from Copper Anode Slimes: A Review of Established Technologies and Current Progress. *Met. Mater. Int.* **2021**, *27*, 2160–2187. [CrossRef]
15. Fernández, M.A.; Segarra, M.; Espiell, F. Selective Leaching of Arsenic and Antimony Contained in the Anode Slimes from Copper Refining. *Hydrometallurgy* **1996**, *41*, 255–267. [CrossRef]
16. Shuiping, Y.; Juner, W.; Huanran, Z.; Hang, C.; Chen, Y. *Furnace Extraction Technology of Copper Anode Slime by Caldo Furnace Method*; Metallurgical Industry Press: Beijing, China, 2019; ISBN 978-7-5024-8038-7.
17. Liu, W. Study on the Treatment of Copper and Lead Anode Sludge by Alkaline Oxidation Method. Ph.D. Thesis, Central South University, Changsha, China, 2011.
18. Xing, W.D.; Lee, M.S. Development of a Hydrometallurgical Process for the Recovery of Gold and Silver Powders from Anode Slime Containing Copper, Nickel, Tin, and Zinc. *Gold Bull.* **2019**, *52*, 69–77. [CrossRef]
19. Hait, J.; Jana, R.K.; Sanyal, S.K. Processing of Copper Electrorefining Anode Slime: A Review. *Miner. Process. Extr. Metall.* **2013**, *118*, 240–252. [CrossRef]
20. Zhou, Y.; Jiang, W.; Guo, X.; Zhao, Y.; Xu, B.; Li, J.; Yang, B. A Selective Volatilization and Condensation Process for Extracting Precious Metals from Noble Lead. *J. Clean. Prod.* **2021**, *294*, 126330. [CrossRef]
21. Zhou, Y.; Jiang, W.; Cha, G.; Deng, J.; Guo, X.; Huang, D.; Xu, B.; Yang, B. Recovery of Associated Precious Metals from By-Products of Lead and Copper Smelting. *Chin. J. Nonferrous Met.* **2021**, *31*, 1–15.
22. Xu, B.; Shi, T.; Yang, B.; Yang, J.; Jiang, W. Research Status on Treatment and Utilization of Arsenic Containing Dust. *J. Kunming Univ. Sci. Technol. (Nat. Sci.)* **2019**, *44*, 1–10.
23. Yang, B.; Xu, B.; Deng, J.; Jiang, W.; Liu, D.; Tian, Y.; Li, Y.; Kong, L.; Yang, J. Method for Recovering Valuable Metal from Copper Anode Slime. Patent 202111191251, 28 December 2021.
24. Li, B.L.; Deng, J.H.; Jiang, W.L.; Zha, G.Z.; Yang, B. Removal of Arsenic, Lead and Bismuth from Copper Anode Slime by a One-Step Sustainable Vacuum Carbothermal Reduction Process. *Sep. Purif. Technol.* **2023**, *310*, 123059. [CrossRef]
25. FactSage Modules. The Equilib Module. Available online: https://www.factsage.com/fs_equilib.php (accessed on 26 April 2023).
26. FactSage Modules. The Phase Diagram Module. Available online: https://www.factsage.com/fs_pd.php (accessed on 26 April 2023).
27. Howard, S.M. Three-Dimensional Predominance Volume Diagrams: The Ni-As-S-O System. *Metall. Mater. Trans. B* **2018**, *49*, 2332–2342. [CrossRef]